Control of spin-polarised currents in graphene nanorings

M. Saiz-Bretín[1], J. Munárriz[1], A. V. Malyshev[1,2], F. Domínguez-Adame[1,3]

[1] *GISC, Departamento de Física de Materiales, Universidad Complutense, E-28040 Madrid, Spain*

[2] *Ioffe Physical-Technical Institute, St-Petersburg, Russia*

[3] *Department of Physics, University of Warwick, Coventry, CV4 7AL, United Kingdom*

Abstract

We study electronic transport in systems comprising square graphene nanorings with a ferromagnetic insulator layer on top of them. The rings are connected symmetrically or asymmetrically to contacts. The proximity exchange interaction of electrons with magnetic ions results in spin-dependent transport properties. When a nanoring is connected asymmetrically, the occurrence of Fano-like antiresonances in the transmission coefficient can induce abrupt changes in the spin polarisation under minute variations of the Fermi energy. We also demonstrate that the spin polarisation can be efficiently controlled by a side-gate voltage. This opens a possibility to use these effects for fabricating tunable sources of polarised electrons.

Keywords: Quantum rings, graphene, spin polarisation, spintronics
PACS: 72.80.Vp, 85.75.Mm, 73.22.−f

1. Introduction

The first direct observation and systematic study of Aharonov-Bohm conductance oscillations through a graphene ring [1] paved the way for exploiting quantum interference effects to design novel nanodevices. In this context, Wu *et al.* have demonstrated theoretically that rectangular graphene nanorings pierced by a magnetic field behave like a resonant tunneling device [2]. Recently, we proposed a novel quantum interferometer based on a hexagonal graphene nanoring [3]. Electron transport in such a device can be controlled by a side gate voltage applied across the nanoring. Its operation does not require a magnetic field and thus it can be more suitable for applications. We

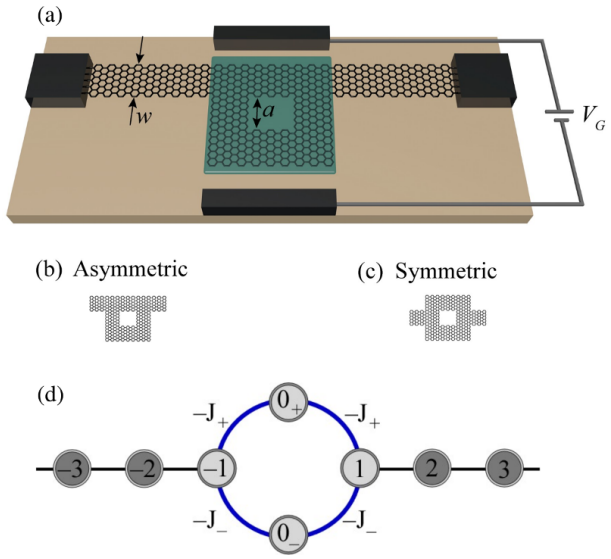

Figure 1: (a) Schematic view of the graphene nanoring with a ferromagnetic layer on top of it (green area). A side-gate voltage can be applied across the ring. The connection between the ring and the GNRs can be (b) asymmetric or (c) symmetric. (d) Schematics of a simple qualitatively equivalent tight-binding lattice model of the ring.

also argued that these systems could be used as spintronic devices if a layer of ferromagnetic insulator, such as EuO, is deposited on top of the ring [4]. Due to the proximity exchange interaction between Eu^{2+} ions and graphene electrons [5, 6] the ring can operate as a spin filter.

In this work we address the spin filtering properties of hybrid systems comprising ferromagnets and square graphene nanorings. In contrast to the previously studied hexagonal nanoring, the type of edge (armchair or zig-zag) of the square nanoring changes at each corner and, more importantly, the connection between the ring and the leads can be symmetric or asymmetric. One of the aims of the work is to compare the transmission properties of both configurations and assess their impact on the performance of the device. Finally, we study the effect of a side-gate voltage applied across the ring and show how the transmission polarisation can be efficiently controlled by varying this voltage.

2. Model and formalism

The square graphene ring is connected symmetrically or asymmetrically to two leads by graphene nanoribbons (GNRs), as shown in Fig. 1. A ferromagnetic layer grown on top of the graphene ring induces spin sublevels splitting due to the proximity exchange interaction [5]. Hereafter we assume the ferromagnet to be EuO because control of spin polarisation was demonstrated experimentally for devices based on this material [6].The two lateral electrodes allow us to apply a side-gate voltage across the ring.

The width of all GNRs is w and the size of the inner hole is $a \times a$. For definiteness, in this work we consider the case $w = a$. The ring is connected to the leads by two armchair GNRs. When the number of hexagons across the GNRs is $N \neq 3n-1$ (n being a positive integer), the GNR band structure has a width-dependent gap and the dispersion relation near the gap is quadratic. Hereafter we will consider only such GNRs because they are believed to be more advantageous for applications [3].

To model the devices we use the following tight-binding Hamiltonian within the nearest-neighbor approximation

$$\mathcal{H} = \sigma\, \Delta_{\rm ex} \sum_{i \in \mathcal{L}} |i\rangle\langle i| - J \sum_{\langle i,j \rangle} |i\rangle\langle j| \ , \tag{1}$$

where $|i\rangle$ is the π-orbital of the i-th carbon atom and the nearest neighbor coupling is $J = 2.8\,\mathrm{eV}$. The ferromagnetic layer affects the site energies of the set $\mathcal{L}$ of carbon atoms which are in contact with it, shifting the energies by the amount $\sigma\Delta_{\rm ex}$, where $\Delta_{\rm ex}$ is the exchange splitting energy and $\sigma = +1$ ($\sigma = -1$) for spin up (spin down) states. Throughout the paper we take $\Delta_{\rm ex} = 5\,\mathrm{meV}$, which is of the order of the values known from the literature for hybrid systems based on graphene and EuO [5, 7, 8].

The quantum transmission boundary method [9, 10] combined with the effective transfer matrix approach [11] were used to calculate wave functions and spin-dependent transmission coefficients $T_\pm$ for spin up (+) and spin down (−) electrons (see Refs. [3] and [4] for further details). We define the degree of transmission polarisation as

$$P = \frac{T_+ - T_-}{T_+ + T_-} \tag{2}$$

and it will be the figure of merit to assess the spin filtering properties of the device.

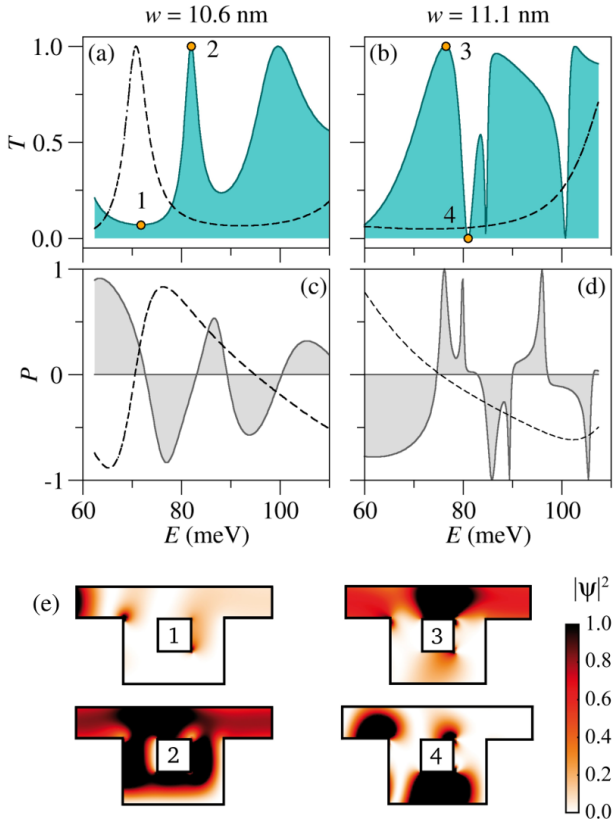

Figure 2: Upper panels show the transmission coefficients in the absence of ferromagnetic layer ($\Delta_{\rm ex} = 0$) for two different values of the GNR width (given in the plot). The transmission polarisation when $\Delta_{\rm ex} = 5\,$meV is shown in the middle panels. Solid and dashed lines correspond to asymmetric and symmetric nanorings, respectively. Lower panels show the density plots of the square modulus of the envelope wavefunction corresponding to the four energies marked by circles in the upper panels.

3. Non-ferromagnetic rings

First, we compare the transmission properties of symmetric and asymmetric nanorings with semiconducting graphene contacts in the absence of proximity exchange interaction ($\Delta_{\rm ex} = 0$) and with zero side-gate voltage ($V_G = 0$). Throughout the paper we focus on the energy region with only one propagating mode in the GNRs, then interference-related effects are not smoothed out due to the superposition of several modes. We have numerically found that the transmission patterns can be grouped into two categories, depending on the value of N. If $N = 3n - 2$ the transmission coefficient presents resonant peaks whose shape is Lorentzian close to the resonance energy. A typical example is shown in Fig. 2(a) corresponding to $w = 10.6\,\mathrm{nm}$ ($N = 43$) for both symmetric (dashed line) and asymmetric (solid line) nanorings. When $N = 3n$ the transmission coefficient strongly depends on the symmetry of the nanoring. As shown in Fig. 2(b) for $w = 11.1\,\mathrm{nm}$ ($N = 45$), the transmission coefficient for symmetrically connected nanorings is rather smooth and increases uniformly in the one-mode energy windows (see dashed line). On the contrary, if the ring is connected asymmetrically, the transmission coefficient presents Fano-like antiresonances (see solid line).

In order to understand the origin of the transmission features, in Fig. 2(e) we plot the square modulus of the envelope wave function for the four energies marked by circles and labelled by numbers in the upper panels of Fig. 2, all of them corresponding to asymmetric rings. When $w = 10.6\,\mathrm{nm}$ ($N = 43$) the electron is strongly backscattered if the energy is far from a resonance ($T \ll 1$) and the corresponding wave function remains in the left contact (state labelled 1). In the case labelled 2 the transmission is large ($T \approx 1$) and the wave function piles up inside the whole nanoring as it happens at resonant transmission. Similar patterns are found for nanorings connected symmetrically. Contrary to that, when $w = 11.1\,\mathrm{nm}$ ($N = 45$) the transmission spectrum has Fano-like features: both resonances with $T \approx 1$ (state 3) and antiresonances with $T = 0$. State labelled 4 represents the latter case: the lower part of the nanoring acts here as a discrete level system at the background continuum of GNR states. At the antiresonance the wave function localizes at the lower arm and is almost zero in the upper arm, which is the typical wave function pattern for Fano antiresonances.

4. Simplified model

Numerical results can be qualitatively explained by a much simpler tight-binding nearest-neighbour lattice model in which the nanoring is represented by a four-site ring connected to semi-infinite chains [see Fig. 1(d) for the schematics]. Upper and lower ring sites, labelled $0_\pm$, have energies $\varepsilon_\pm$ while all other site energies are zero. Adjacent ring sites are coupled with hopping integrals $-J_\pm$ while the rest of hopping integrals are equal; their value is used as the energy unit.

The transmission coefficient in this simplified model is

$$T(E) = \frac{4 - E^2}{4 - E^2 + F^2(E)} \ , \quad F(E) = \left(\frac{J_+^2}{E - \varepsilon_+} + \frac{J_-^2}{E - \varepsilon_-} \right)^{-1} - E \ . \quad (3)$$

Let us first consider a symmetric ring for which $\varepsilon_+ = \varepsilon_- \equiv \varepsilon$, $J_+ = J_- \equiv J$ and $F(E) = E(1/2\,J^2 - 1) - \varepsilon/2J^2$. When $2J^2 \neq 1$, the real part of the transmission amplitude vanishes at the resonance energy $E_r = \varepsilon/(1 - 2J^2)$. In this case, the transmission coefficient shows a Lorentzian profile close to the resonance energy given by

$$T(E) = \frac{\Gamma^2}{\Gamma^2 + (E - E_r)^2} \ , \quad \Gamma^2 = \frac{1 - E_r^2/4}{(J^2/2 - 1)^2} \ . \quad (4)$$

This profile is consistent with the numerical profiles found in symmetric nanorings with $N = 3n - 2$ and shown in Fig. 2(a). Notice that the simplified model shows no resonances when E_r lies outside the band of the contact, which is in qualitative agreement with the smooth behavior of the transmission coefficient of symmetric nanorings with $N = 3n$ shown in Fig. 2(b).

Next, we consider an asymmetric ring where ε_+ and ε_- are different. The most salient feature in this case is the vanishing of the transmission at the antiresonance energy

$$E_a = \frac{\varepsilon_- J_+^2 + \varepsilon_+ J_-^2}{J_+^2 + J_-^2} \ . \quad (5)$$

This result qualitatively reproduces the dips observed in Fig. 2(b) (see, e.g., antiresonance labelled 4). In addition, when E_a lies outside the band of the semi-infinite chains there are no antiresonances in the transmission coefficient. This prediction also agrees well with the results corresponding to $N = 3n - 2$, shown in Fig. 2(a).

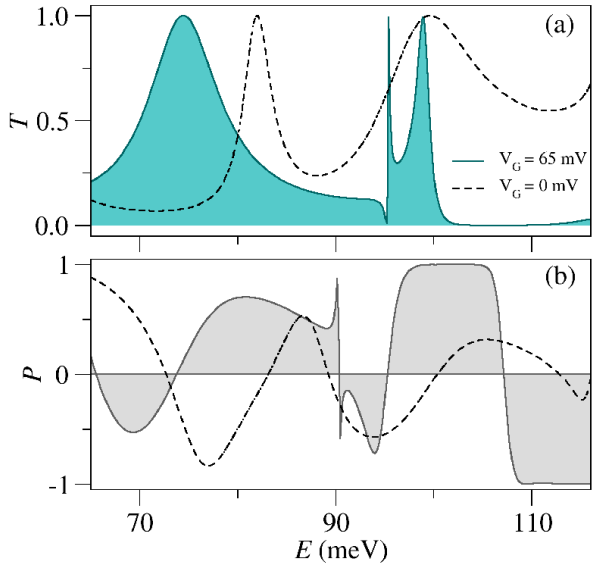

Figure 3: Upper panel shows the transmission coefficient in the absence of ferromagnetic layer ($\Delta_{\rm ex} = 0$) for an asymmetric ring with $w = 10.6\,$nm. The transmission polarisation when $\Delta_{\rm ex} = 5\,$meV is shown in the lower panel. Solid and dashed lines correspond to an applied side-gate of $V_G = 65\,$mV and $V_G = 0$, respectively.

5. Ferromagnetic rings

When a EuO layer is deposited on top of the nanoring, the interaction with the ferromagnet shifts the transmission curves towards upper/lower energies for spin up/down electrons. Except for the energy shift, the transmission patterns remain qualitatively the same and are not shown here, while the transmission polarisations P are presented in the middle panels of Fig. 2. For symmetrically connected nanorings, P changes sign smoothly over a wide energy region. Consequently, transmission polarisation remains rather insensitive to changes of the Fermi energy. On the contrary, the polarisation for asymmetrically connected nanorings changes more abruptly, especially when the transmission coefficient shows Fano-like antiresonances, as is the case of $N = 3n$. Therefore, asymmetric rings seem to be more promising from the point of view of device applications since minute variations of the Fermi energy can lead to large changes in the spin polarisation.

However, both configurations (symmetric and asymmetric) show a similar behavior when a side-gate voltage V_G is applied across the ring. Therefore, we will only consider one of the rings hereafter, namely the asymmetric ring with $w = 10.6\,\mathrm{nm}$ ($N = 43$). As shown in Fig. 3(a), new sharp features can be induced in the transmission coefficient by the side-gate, as the ones found around $E = 95 - 100\,\mathrm{meV}$. These strong asymmetries result in a more abrupt change of the polarisation when varying the Fermi energy [see Fig. 3(b)]. In addition, the side-gate plays another important role as it allows for a precise control of the transmission polarisation through the device. Fig. 4(a) shows the polarisation map as a function of the carrier energy E and the side-gate voltage V_G. As the figure suggests, the sign of the polarisation can be changed by the side gate. We define the average polarisation as follows

$$\langle P\rangle = \frac{\langle T_+\rangle - \langle T_-\rangle}{\langle T_+\rangle + \langle T_-\rangle}\ , \quad \langle T_\pm\rangle = \frac{1}{E_2 - E_1}\int_{E_1}^{E_2} T_\pm(E)\,dE\ . \tag{6}$$

Note that $\langle P\rangle$ gives the average electric current polarisation at zero temperature when Fermi levels of the two contacts are set to E_1 and E_2. The average polarisation $\langle P\rangle$ is plotted as a function of V_G in Fig. 4(b) for $E_1 = 103.9\,\mathrm{meV}$ and $E_2 = 108.4\,\mathrm{meV}$. The figure shows that in the vicinity of the gate voltage $V_G \approx 70\,\mathrm{mV}$ the polarisation undergoes an abrupt change from $\langle P\rangle \approx 0.9$ to $\langle P\rangle \approx -0.8$, suggesting the possibility of controlling the electric current polarisation by the side gate voltage.

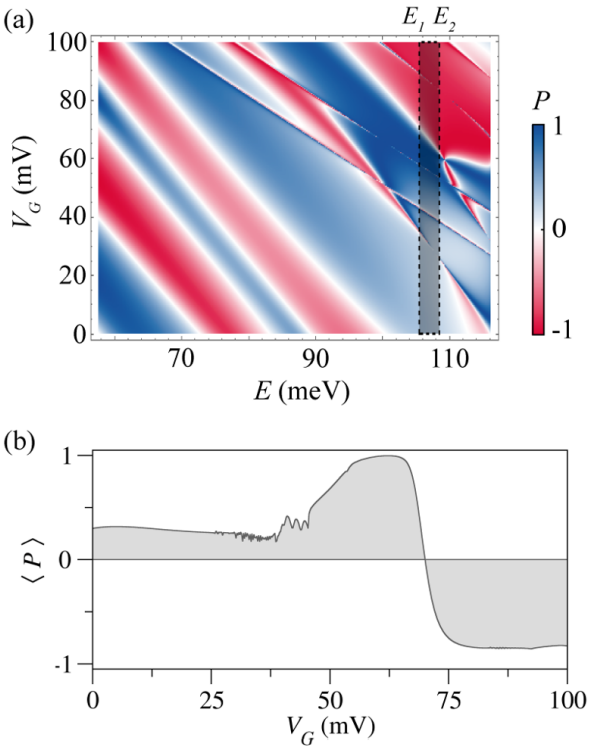

Figure 4: (a) Transmission polarisation as a function of the carrier energy E and the side-gate voltage V_G. (b) Average transmission polarisation $\langle P \rangle$ as a function of V_G calculated for $E_1 = 103.9\,\mathrm{meV}$ and $E_2 = 108.4\,\mathrm{meV}$ (see Eq. (6) and the text).

6. Conclusions

In summary, we have proposed and studied a novel spin filter system which exploits quantum interference effects. The device comprises a square graphene nanoring, connected symmetrically or asymmetrically to the leads, and a ferromagnetic layer (e. g. of EuO) grown on top of the ring. The proximity induced exchange interaction between the ferromagnetic ions and the graphene electrons result in a spin-dependent transmission coefficient and, as a consequence, a spin-dependent conductance and electric current. We showed that the polarisation of the transmission changes abruptly when the Fermi energy is varied in the vicinity of Fano-like antiresonances which occur in asymmetrically connected nanorings. We put forward and analysed a simplified quasi-one-dimensional model of the nanoring and explained qualitatively different typical transmission features found in both symmetrically and asymmetrically connected nanorings. We also demonstrated that the side-gate voltage can be used to control the transmission polarisation in an efficient way in all the studied cases (independently of the width of the GNRs or the symmetry of the system geometry). The side-gate gate voltage induces Fano-like antiresonances in rings with both types of connections and leads to more abrupt polarization variations in a controllable way. It should be mentioned that Fano-like antiresonances can also be induced by a magnetic flux [12] but spin control by electric means is more suitable for nanoelectronic applications. Therefore, we conclude that the predicted effects open a possibility to design novel tunable sources of polarised electrons.

F. D-A. thanks the Theoretical Physics Group of the University of Warwick for the warm hospitality and the Spanish Ministry of Education (grant PRX14/00129). This work was supported by MINECO (project MAT2013-46308). A. V. M. was partially supported by CAPES (grant PVE-A121).

[1] S. Russo, J. B. Oostinga, D. Wehenkel, H. B. Heersche, S. S. Sobhani, L. M. K. Vandersypen, A. F. Morpurgo, Phys. Rev. B 77 (2008) 085413.

[2] Z. Wu, Z. Z. Zhang, K. Chang, F. M. Peeters, Nanotech. 21 (2010) 185201.

[3] J. Munárriz, F. Domínguez-Adame, A. V. Malyshev, Nanotech. 22 (2011) 365201.

[4] J. Munárriz, F. Domínguez-Adame, P. A. Orellana, A. V. Malyshev, Nanotech. 23 (2012) 205202.

[5] H. Haugen, D. Huertas-Hernando, A. Brataas, Phys. Rev. B 77 (2008) 115406.

[6] A. G. Swartz, P. M. Odenthal, Y. Hao, R. S. Ruoff, R. K. Kawakami, ACS Nano 6 (2012) 10063.

[7] J. Zou, G. Jin, Y.-Q. Ma, J. Phys.: Condens. Matter. 21 (2009) 126001.

[8] Y. Gu, Y. H. Yang, J. Wang, K. S. Chan, J. Appl. Phys. 105 (2009) 103711.

[9] C. S. Lent, D. J. Kirkner, J. Appl. Phys. 67 (1990) 6353.

[10] D. Z.-Y. Ting, E. T. Yu, T. C. McGill, Phys. Rev. B 45 (1992) 3583.

[11] J. Schelter, D. Bohr, B. Trauzettel, Phys. Rev. B 81 (2010) 195441.

[12] D. Faria, R. Carrillo-Bastos, N. Sandler, A. Latg, J. Phys.: Conden. Matter 27 (2015) 175301.